Investigation of the tribological behavior of chromium aluminum silicon nitride coatings via both scratch sliding test and FEM simulation

Cite as: AIP Advances **9**, 025116 (2019); https://doi.org/10.1063/1.5085373
Submitted: 12 December 2018 . Accepted: 11 February 2019 . Published Online: 21 February 2019

Zhitong Chen, Guangjian Peng, Peijian Chen, Yuan Xia, and Guang Li

Investigation of the tribological behavior of chromium aluminum silicon nitride coatings via both scratch sliding test and FEM simulation

Cite as: AIP Advances 9, 025116 (2019); doi: 10.1063/1.5085373
Submitted: 12 December 2018 • Accepted: 11 February 2019 •
Published Online: 21 February 2019

Zhitong Chen,[1,2,3] Guangjian Peng,[4,a)] Peijian Chen,[5] Yuan Xia,[1,2] and Guang Li[1,2,a)]

AFFILIATIONS

[1]Institute of Mechanics, Chinese Academy of Sciences, Beijing 100190, China
[2]University of Chinese Academy of Sciences, Beijing 100049, China
[3]Department of Mechanical and Aerospace Engineering, George Washington University, Washington, DC 20052, USA
[4]College of Mechanical Engineering, Zhejiang University of Technology, Hangzhou 310014, China
[5]State Key Laboratory for Geomechanics and Deep Underground Engineering, School of Mechanics and Civil Engineering, China University of Mining and Technology, Xuzhou 221116, China

[a)]**Corresponding Author: E-mail address:** penggj@zjut.edu.cn, *lghit@imech.ac.cn*

ABSTRACT

The finite element method (FEM) and scratch sliding test were combined to investigate the tribological behaviors of Chromium Aluminum Silicon Nitride (CrAlSiN) coatings with various Si contents. The tribological behavior was evaluated through sliding tests using a conventional ball-on-disc wear apparatus. It was found that the coefficient of friction (COF) of CrAlSiN was lower than CrAlN coating and it reached a minimum value of 0.56 for $CrAlSi_{3.7}N$. Energy-dispersive Scanning Electron Microscopy (SEM) with X-ray spectroscopy (EDX) was employed to reveal the compositions of wear debris formed during the scratch sliding experiments. As a reasonable approximation, a static condition was applied, and the scratch behavior was modeled by a sphere indenter scratching on a thin coating coated on a thick substrate. A three-dimensional finite element model was constructed with the help of the ABAQUS to describe the mechanical response during scratch.

I. INTRODUCTION

Chromium nitride coatings have high hardness as well as good wear resistance due to its low COF, and they have been widely used as protective coatings for various tribological forming and casting applications.[1,2] To further extend the functionality and performance, the material properties have been modified to overcome related deficiencies. In recent years, many researchers dope the third element (such as Al, B, Ti, W, etc.) in binary CrN system to improve mechanical, thermal and anticorrosion behaviors.[3–6] Among these coating systems, CrAlN stands to be a promising candidate due to its favorable oxidation resistance and thermal stability.[7,8] Moreover, adding silicon to transition metal nitrides has been reported to significantly improve several mechanical properties, including hardness, toughness and oxidation resistance.[9,10] Therefore, CrAlSiN coatings are of superhardness, excellent oxidation resistance and wear resistance due to the substitutional replacement of the smaller Si and Al atoms into the Cr sites. Mo et al. and Geng et al. studied tribological behaviors of CrAlN and CrSiN, respectively.[11,12] Some work focused on tribological behavior of nanocomposite structure of CrAlSiN coatings.[13–17]

The relative slippage on a contact surface in the Coulomb friction theory initiates when the magnitude of the friction stress vector arrives at the critical value $\mu\sigma_n$, where σ_n is the normal contact stress and μ is the Coulomb friction coefficient.[18,19] The scratch COF μ_s is obtained by the ratio of

tangential force F_t to the normal force F_n. Due to deformations of the surface coating, F_t is not only from shear stress but from a part of critical normal stress σ_n. In addition, a part of F_n also comes from shear stress. They cause the scratch friction coefficient μ_s to be a sum of Coulomb friction coefficient μ and deformation friction coefficient μ_d. In comparison with the Coulomb friction coefficient μ, deformation friction coefficient μ_d is negligible under a slight deformation of coatings and is comparable and even larger under a serious deformation. With the absence of stress and strain filed, it is difficult to measure μ_d and further μ_s that depends μ_d) is not very understandable. In some cases, when friction stress on a contact surface reaches material yield strength in shear τ_y, contact slippage could take place even if the slipping condition for Coulomb friction is not satisfied.[20–23] As a result, the scratch coefficient μ_s is not a simple addition of the surface deformation coefficient μ_d and the traditional Coulomb friction coefficient μ but depends on three variables: μ, μ_d and τ_y. Without the knowledge of stress field, it is unclear whether the plastic slippage occurs. The finite element method is an important tool to describe the mechanical responses in the scratch process.[24,25]

In this present work, the CrAlSiN coatings with different Si content (0, 3.7 at. %, 6.3 at. %, 8.6 at. %, 10.7 at. % and 13.1 at. %) were deposited to study tribological behaviors during scratch. Consequently, the main aim of this work was to systematically investigate and elucidate in detail the effects of various Si contents on the tribological performances via experiment and modeling.

II. EXPERIMENT AND NUMERICAL PROCEDURE

The CrAlSiN coatings investigated in this research were deposited on Cu, HSS and Si wafer substrates using medium frequency pulse magnetron sputtering technique. The CrAlSiN coatings were deposited on Cu for EDX experiments, on Si wafer for microstructure experiments, on HSS for mechanical and tribological experiments. Customized Cr and AlSi with different Si content targets in a reactive nitrogen atmosphere were used to obtain coatings with an increasing Si content (as shown in Table I). The HSS substrates of the disc type (30 mm in diameter and 5 mm in thickness) were cleaned in an ultrasonic cleaner using acetone and alcohol for 20 min. Mirror-polished Si and polished Cu substrate were cleaned separately in an ultrasonic cleaner using acetone and alcohol for 2 min and 20 min, respectively. The substrates were cleaned again by ion bombardment using a bias voltage of –900 V under Ar atmosphere of 1.5 Pa for 15 min. Substrate bias voltage of -150 V and ratio N_2/Ar of 1:2 were used. The coatings were deposited from sputter sources at a working pressure of 0.5 Pa and the input power on the CrAl(Si) target was fixed at 250W. The background pressure of our apparatus was 5×10^{-5} Pa.

TABLE I. Chemical composition of CrAlSiN films.

Target	Elements (at. %)			
	Cr	Al	Si	N
Al + Cr + Al	20.1	29.4	0.0	50.5
Al + Cr + $AlSi_{10}$	18.0	29.2	3.7	49.1
$AlSi_{10}$ + Cr + $AlSi_{10}$	17.9	26.8	6.3	49.0
Al + Cr + $AlSi_{30}$	17.6	23.4	8.6	50.4
$AlSi_{10}$ + Cr + $AlSi_{30}$	16.1	21.3	10.7	51.9
$AlSi_{30}$ + Cr + $AlSi_{30}$	18.9	19.5	13.1	48.5

The morphology of coating was observed also by a field-emission scanning electron microscopy (SEM, FEI Sirion400NC). Chemical analysis was performed on a field emission scanning electron microscope equipped with INCA energy-dispersive X-ray spectroscopy (EDX). The crystallographic investigations were performed by glancing angle X-ray diffraction (GAXRD, X'Pert PRO MPD) under 2θ mode. The X-ray was generated from a Cu target operated at 40 kV and 150 mA. The 2θ scanning range was from 30° to 80°. The scratch sliding tribological tests of CrAlSiN coatings with different Si content were performed on a conventional ball-on-disc rotational wear apparatus to evaluate the friction coefficient and wear behaviors. A ZrO_2 ball was used as a counterpart material. The sliding distance is around 560 meters. The tests were conducted with a sliding speed of 0.088 m/s under a load of 1 N at ambient temperature (around 25°C) and relative humidity (25-30% RH) condition. SEM was employed to observe the morphology of the wear track after each sliding experiment. Energy dispersive spectroscopy (EDS) was used to reveal the compositions of wear debris.

In the finite element model, the radius of spherical indenter was R = 3170 μm, and thickness of coating was h = 3 μm consistent with experiments. The thickness of the sample used in simulations is 150 μm (in spite of 5 mm in experiments) because the results show that stresses and strains were zero in the region ($z < -100\ \mu m$) and that further increasing the thickness of the substrate did not cause any effect. In the current simulations, 700 μm was used for the length and 360 μm was used for the width. The extra loadings were applied by following two steps: first, the indenter was compressed down to the coated surface by the normal force F_n = 1N; and second, a tangential displacement loading was applied to keep the indenter sliding along x-axis at the fixed F_n. The boundary conditions were as follows: 1) Coulomb friction was applied on the contact surface between the indenter and the coating; 2) complete cohesion was employed on the contact surface between coating and substrate; and 3) the other surfaces of the coating and substrate were fixed.

III. EXPERIMENTAL RESULTS AND DISCUSSION

A. Cross-sectional micrographs

Fig. 1 shows the cross-sectional micrographs of CrAlSiN coatings with different Si content. The columnar crystals growth direction of coatings is perpendicular to the coating surface. Fig. 1 markedly shows a serial conversion of microstructure with Si content. The insertion of Si into nitride coatings may improve the densification of coating and reduce the grain size of columnar coatings.[26] The columnar structure of the CrAlN coating switches to spherical and equiaxial

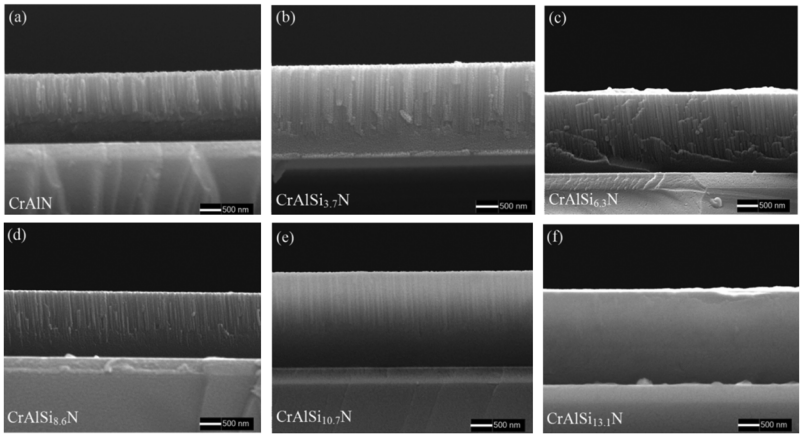

FIG. 1. Cross-sectional SEM images of CrAlSiN coatings with various Si content (0.0, 3.7 at. %, 6.3 at. %, 8.6 at. %, 10.7 at. %, and 13.1 at. %).

grains with 13.1 at. % Si content. In our previous studies,[27] a retardation of the columnar growth by the addition of Si was verified from the elimination of (111) preferred orientation (no diffraction peaks of SiN_x) and the hardness of CrAlSiN coatings exhibited the maximum hardness value at Si content approximate 8.6 at. % due to the microstructural change to crystal size refinement as well as solid-solution hardening.

B. XRD results

The X-ray diffraction patterns of CrAlSiN films are shown in Fig. 2. The substitutional replacement of the smaller Al and Si atoms into the Cr sites led to peaks falling between those for B1 AlN and B1 CrN.[28] From this experiment and other studies,[29] c-CrAlN was confirmed. From the presence of (111), (200), (220) and (311) peaks, the B1 NaCl-type fcc structure of the films was identified. No diffraction peaks of Si_3N_4 were found in this pattern so that its amorphous feature was confirmed on the basis of literature data.[30] In addition to peak positions, it was noted that the diffraction intensity of (111) peak gradually reduced with the increasing Si content in the CrAlSiN films

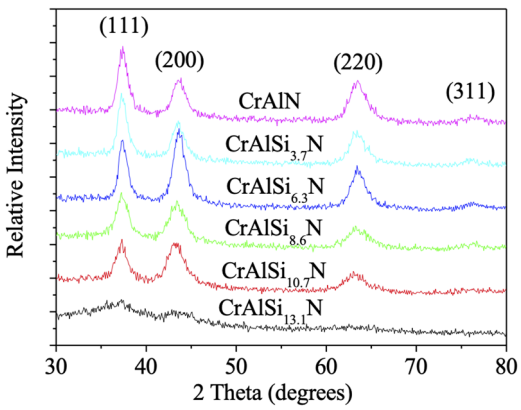

FIG. 2. XRD pattern of CrAlSiN with different Si content.

while (200) peak firstly increased and then reduced. Variations of the orientations for the fcc films, such as CrN, were interpreted on the basis of surface and strain energy.[31] To minimize the increasing strain and stress during the depositing process, the fcc film tended to grow along the direction with lowest strain energy. From the XRD pattern, it was found that the preferable growth along the (111) direction would be interrupted by the formation of amorphous Si_3N_4 in CrAlSiN films. Grain growth along the (200) direction, which possessed the lowest surface energy, and fine-grain structure were expected in the CrAlSiN coatings due to the incorporation of amorphous Si_3N_4 phase. Fig. 1 presents the cross-sectional images of CrAlSiN films, which also supported the presumptions from XRD patterns. The fine-grain structure of the CrAlSiN films was also revealed. From the results of the XRD patterns and cross-sectional images, retardation of columnar growth by incorporation of Si into the CrAlN coating is evident.

C. Mechanical and tribological behaviors

Hardness, COF, and SEM wear tracks morphologies of CrAlSiN against ZrO_2 ball at room temperature as a function of Si contents are shown in Fig. 3. As the Si content increased in the coatings, the hardness of the CrAlSiN films gradually increased from Hv1348 for CrAlN, reached maximum hardness value of Hv2343 at the Si content of around 8.6 at.%. However, the hardness of CrAlSiN films reduced with further increase in Si content. Both XRD and SEM showed that Si had a grain refining effect in the CrAlN. The large increase in the hardness value of CrAlSiN films at the Si content of around 8.6 at.% can be explained with a grain boundary hardening phenomenon derived from crystal size refinement.[32] Another possible mechanism would be the solid-solution hardening of crystallites by Si dissolution into CrAlN. Furthermore, when the Si content in the films was more than 9 at.%, presence of the Si_3N_4 phase was amorphous.[28] When the amorphous phase became thicker than crystallites, the hardness of coatings became strongly dependent on the property of the amorphous phase.[30] In the dry sliding tests, the COF for the coatings against ZrO_2 balls were measured. All specimens exhibited

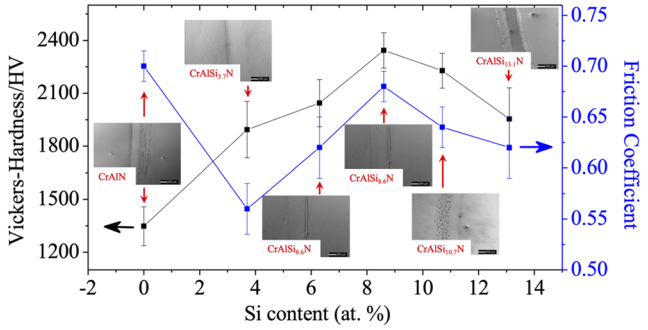

FIG. 3. Hardness, COF, and SEM wear tracks morphologies of CrAlSiN against ZrO_2 ball at room temperature as a function of Si contents (0.0, 3.7, 6.3, 8.6, 10.7, and 13.1%).

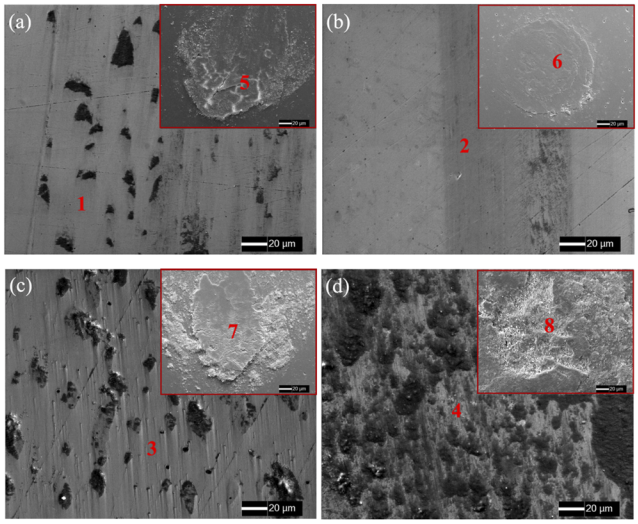

FIG. 4. Local wear tracks morphologies of CrAlN (a), $CrAlSi_{3.7}N$ (b), $CrAlSi_{8.6}N$ (c) and $CrAlSi_{13.1}N$ (d) coatings. Wear scar morphologies of ZrO_2 ball (in red box) against CrAlN (a), $CrAlSi_{3.7}N$ (b), $CrAlSi_{8.6}N$ (c) and $CrAlSi_{13.1}N$ (d) coatings.

low values of COF at the initial running-in stage. The COF increased gradually as the sliding distances increased until stable stage was reached. The COF of CrAlN coating was higher than that of the CrAlSiN coatings, therefore Si dissolution into CrAlN led to decreased in COF. In CrAlSiN coatings, the lowest COF of 0.56±0.03 for CrAlSiN coating with Si addition approximate 3.7 at.% was observed. As the Si content increased in the coatings, the COF gradually increased to maximum value of 0.68±0.02 at the Si content of approximate 8.6%. However, the COF of CrAlSiN coatings reduced with further increase in the Si content. The coating surfaces after sliding wear against ZrO_2 balls were examined using SEM. Wear tracks were observed on all six coatings against ZrO_2 sliding balls as shown in Fig. 3. There were some ploughs and debris on CrAlN coating. In CrAlSiN coatings when Si ≤6.3 at. %, the wear tracks of coatings were very smooth. When the Si content was further increased, ploughs and debris appeared, and the diameter of debris increased. The CrAlSiN coating was worn at the Si content of approximate 13.1 at. %.

Local wear tracks morphologies of CrAlN, $CrAlSi_{3.7}N$, $CrAlSi_{8.6}N$ and $CrAlSi_{13.1}N$, and wear scar morphologies of ZrO_2 ball against CrAlN, $CrAlSi_{3.7}N$, $CrAlSi_{8.6}N$ and $CrAlSi_{13.1}N$ coatings are shown in Fig. 4. The compositions of wear tracks were analyzed by EDS to determine the products of friction and results were given in Table II. In Fig. 3 and 4, the $CrAlSi_{3.7}N$ coating had a much smoother wear track than other coatings. As shown on the wear track by EDS results of $CrAlSi_{3.7}N$ coating, the oxygen content was much lower in regions 2 than in regions 1, 3 and regions 4. For $CrAlSi_{13.1}N$ coating, it was worn out but there was still CrAlSiN coating. Because the hardness of $CrAlSi_{13.1}N$ coating is much higher than HSS substrate, the detached coating was crushed into fine particles, a process that led to the formation of deep pits. In all EDS results, there was no Zr found in all wear tracks. EDS results of wear scars of ZrO_2 balls against six different Si content showed that there was no Zr composition. Therefore, chemical products generated during wear were transferred from coatings to ZrO_2 balls and then deposited on them. Cracks and detached debris appeared in the wear scar of ZrO_2 ball against CrAlN coating. However, chemical products generated during wear on ZrO_2 balls against $CrAlSi_{3.7}N$ and $CrAlSi_{6.3}N$ coatings were dense and there were no cracks. Chemical products generated during wear had detached ZrO_2 balls against $CrAlSi_{8.6}N$ and $CrAlSi_{10.7}N$ coatings at relatively high proportion. For ZrO_2 ball against $CrAlSi_{13.1}N$ coating, there was a high amount of Fe and a relatively low amount of Al. When the Si content was ≤ 8.6 at. %, the Al content of ZrO_2 balls reduced with increasing Si content and reached a maximum content value of 58.5 at. % at the Si content of 3.7 at. %. However, the content of Al on ZrO_2 balls increased with further increase in the Si content.

The high hardness of CrAlSiN coatings prevented significant plastic deformation under contact stress in the friction process of coating so that it avoided serious ploughs. Therefore, CrAlSiN coatings had an excellent dry sliding and wear resistance. In CrAlSiN coatings, the content of amorphous SiN_x phase increased with increasing Si content, while amorphous SiN_x phase was much softer than the CrN phase. These results show that coatings can easily produce detached debris under friction force and contact stress in friction process (Fig. 4). As the Si content increased in the coatings, the tribological mechanism changed from abrasive wear to fatigue

TABLE II. EDX results of coatings from point 1 to point 8 in Fig. 4.

Element [%]	Cr	Al	Si	N	O	Fe
Spectrum 1	16.2	20.5	0.0	49.5	13.3	0.5
Spectrum 2	18.3	22.7	3.5	49.3	5.8	0.4
Spectrum 3	17.5	19.8	8.6	45.1	8.6	0.4
Spectrum 4	4.7	5.7	2.3	10.4	19.3	63.3
Spectrum 5	66.1	10.6	0.00	4.0	18.6	0.7
Spectrum 6	0.2	58.5	2.3	4.6	34.2	0.2
Spectrum 7	13.2	40.5	6.3	3.1	36.8	0.1
Spectrum 8	0.7	47.3	9.5	0.1	38.5	3.9

wear. Both CrAlN and CrAlSiN (≥8.6 at. %) coatings belonged to fatigue wear. Lower Si content (≤6.3 at. %) CrAlSiN coatings had higher oxidation resistance in friction process (Table II), which indicates that the tribological mechanism of low Si content coatings was not fatigue wear but abrasive wear. The wear scar EDX results of wear scar on the ZrO_2 balls showed that Al content in wear scars on the ZrO_2 ball against $CrAlSi_{3.7}N$ coating was highest and against CrAlN coating was lowest. As the Si content increased to 8.6 at. % in the CrAlSiN coatings, Al content in wear scar on the ZrO_2 ball was reduced. Alumina was known to have lower COF than chromium oxide.[33] Therefore, the COF of CrAlN was higher than that of CrAlSiN and the COF of CrAlSiN increased as Si content increased up to approximate 8.6 at. %. When the content of Si exceeds 9 at. %, the properties of CrAlSiN coatings depended on amorphous Si_3N_4 (as shown in Fig. 2). In friction process amorphous Si_3N_4 and SiO_2 phases existed on the surface of CrAlSiN coatings, which would be also caused by following tribochemical reactions between Si and ambient humidity.[33] The products of SiO_2 and Si $(OH)_4$ were known to play a role as a self-lubricating layer. Therefore, the COF of CrAlSiN reduced with Si content increasing when Si > 8.6 at. %. This was another reason for CrAlN coating having highest COF.

IV. NUMERICAL SIMULATIONS ON TRIBOLOGICAL BEHAVIORS

With the absence of a stress-strain field it is difficult to describe the tribological behavior between the spherical indenter and surface coatings. In this section, a three-dimensional finite element model was proposed to elucidate material mechanical responses during the scratch with the help of the finite element code ABAQUS.

A. Numerical model

In one revolution of the indenter on the coatings, the magnitudes of the applied tangent and normal forces were constant in the ball-on-disc wear apparatus. As a reasonable approximation, a static condition was applied, and the scratch behavior was modeled by a sphere indenter scratching on a thin coating coated on a thick substrate as shown in Fig. 5.

As in pioneering research (e.g. in Ref. 34,35), the indenter was also accepted as a rigid body, and the effect of this condition would be discussed. The deformations of the coating and substrate were described by the position vector of the particle in the deformed state $\boldsymbol{r} = \boldsymbol{r}(\boldsymbol{r}_0, t)$, which was a function of its initial position vector $\boldsymbol{r}_0$ in the undeformed configuration and time t. The multiplicative decomposition of the deformation gradient $\boldsymbol{F} = \partial \boldsymbol{r}/\partial \boldsymbol{r}_0 = \boldsymbol{V}_e \cdot \boldsymbol{F}_P$ into symmetric elastic stretch tensor V_e and plastic F_P contributions was used. While we utilized the small elastic strain assumption: $\boldsymbol{\varepsilon}_e = \boldsymbol{V}_e - \boldsymbol{I}$ ($\boldsymbol{I}$ is the second-rank unit tensor), plastic strains and material rotations could be large. A total system of equations for the problem of linearly-elastic, perfectly-plastic flow in the coating and substrate was used as follows:

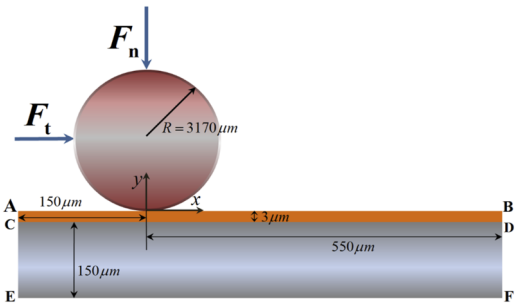

FIG. 5. Schematic representation of the scratch process on a coated substrate.

The deformation rate $\boldsymbol{d} = (\dot{\boldsymbol{F}} \cdot \boldsymbol{F}^{-1})_s$ was decomposed into elastic (subscript e) and plastic (subscript p) components:

$$\boldsymbol{d} = \overset{\nabla}{\boldsymbol{\varepsilon}_e} + \boldsymbol{d}_p. \tag{1}$$

Hooke's law for volumetric and deviatoric parts of the Cauchy stress $\mathbf{T}$:

$$p = -\frac{\sigma_{xx} + \sigma_{yy} + \sigma_{zz}}{3} = -K\varepsilon_v; \quad \boldsymbol{s} = 2G dev\boldsymbol{\varepsilon}_e. \tag{2}$$

Von Mises yield condition:

$$\sigma_i = \left(\frac{3}{2}\boldsymbol{s} : \boldsymbol{s}\right)^{0.5} \le \sigma_y \tag{3}$$

In the elastic region:

$$\sigma_i < \sigma_y \rightarrow \boldsymbol{d}_p = 0 \tag{4}$$

Plastic flow rule in the plastic region:

$$\sigma_i = \sigma_y \rightarrow \boldsymbol{d}_p = \lambda \boldsymbol{s}; \quad \lambda \ge 0 \tag{5}$$

Equilibrium equation:

$$\nabla \cdot T = 0 \tag{6}$$

where $\overset{\nabla}{\boldsymbol{\varepsilon}_e}$ is the Jaumann objective time derivative of the elastic strain; p is the pressure; $\boldsymbol{s}$ is the deviator of the Cauchy stress tensor $\mathbf{T}$, $\boldsymbol{s} = dev\mathbf{T}$; ε_v is the elastic volumetric strain; K and G are the bulk and shear moduli respectively; σ_i is the effective stress; σ_y is material yield strength; and the parameter λ is iteratively updated by satisfaction of the von Mises yield criteria in Eq. (3). Material parameters (K, G, and σ_y) have different values for the coating and the substrate.

The following material properties are used for the coating:[36,37] yield strength σ_{y1} = 9.5 GPa (CrAlN) and 15.3 GPa ($CrAlSi_{8.6}N$), Young's modulus E_1 = 341 GPa (CrAlN) and 500 GPa ($CrAlSi_{8.6}N$); and for the HSS substrate: σ_{y2} = 4.1 GPa and E_2 = 200 GPa. Poisson's ratio almost does not affect tribological behaviors (see Ref. 38) and is taken as v = 0.3 for both coating and substrate. Coulomb friction coefficient is taken as μ = 0.3.

B. Numerical results and discussions

Due to symmetry of the plane z = 0, which went through the center of the spherical indenter (see in Fig. 5), the results for half of the indenter-coating-substrate structure with $z \le 0$ would be presented. Since the simulation was done for half

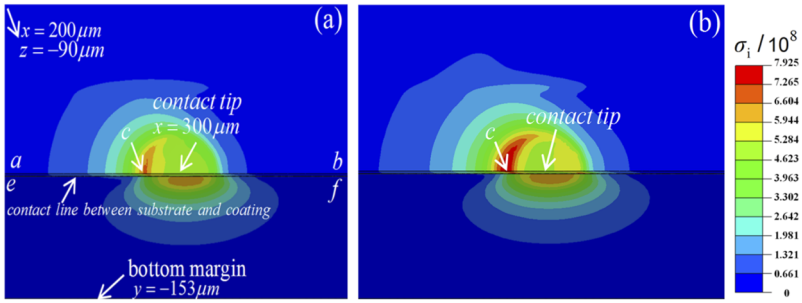

FIG. 6. The distribution of the effective stress σ_i on the coating and substrate in the current configuration for (a) CrAlN and (b) $CrAlSi_{8.6}N$ with the same region. Curve line *ab* was the on *x*-axis in the undeformed configuration, and Curve *ef* was the contact line between substrate and coating and with $y = -3\mu m$ and $z = 0$ in the undeformed configuration. Point *c* was on the curve *ab* and is the cut-off point between contact and noncontact for the indenter and coating.

of the structure, a new boundary condition would be applied: there was no displacement along the *z*-axis ($\mu_3 = 0$) on the symmetry plane $z = 0$. To exclude the effect of the initial indentation, all results would be extracted at the slippage distance of the indenter 300 μm, which meant that the indenter's tip in Fig. 5 slides to the position $x = 300$ μm. Fig. 6 represents the distribution of the effective stress σ_i on the contact surface. For the CrAlN coating the effective stress was much smaller than the material yield stress σ_y, which indicated that the material completely elastically deformed and plastic deformation did not exist. Different from Ref. 39, the residual stress was not observed in Fig. 6, because in addition to the absence of plastic deformation, elastic deformation in the current model was very small in the contact region and the region far from the contact region material deformation could automatically disappear. Without plastic deformation, plastic sliding in Ref. 21, 22 also did not occur and classic elasticity laws without considering size effects by plastic strain gradient theories (see Ref. 40) was reasonable for the current model. As long as it is larger than the effective stress the magnitude of yield strength does not affect the deformation at all. When the yield strength is accepted as one third of the material hardness,[41] the magnitude of material hardness does not result in the difference on the scratch friction coefficient in Fig. 3. Consequently, the distinctions of the stress-strain field between CrAlN and $CrAlSi_{8.6}N$ were only determined by Young's modulus. With the increased in Young's modulus from CrAlN to CrAlSiN, material became harder and more difficult to deform elastically. Under the fixed normal force $F_n = 1$ N ($F_n = 0.5$ N for a half of structure), the CrAlN coating was easily deformed, leading to a less stress concentration in comparison with CrAlSiN (Fig. 6). The region with large effective stress was localized at the right contact boundary in the neighborhood of point *c*, due to a large tensional stress σ_{xx}. This tensional stress was due to the large tangential friction stress at the content region. If a very large normal force F_n was applied to cause a severe plastic deformation, the largest effective stress would not occur in the neighborhood of point *c*, because a large F_n caused a compressive stress σ_{xx} during the extrusion of the material, which compensated the tensional stress σ_{xx} due to the friction stress. A complete cohesion condition was used on the contact region between the coating and substrate, which meant that the displacement was continuous but the effective stress was not continuous due to different Young's moduli (while normal and shear stresses are continuous).

The distribution of the displacement along the *y*-axis u_2 is shown in Fig. 7 for CrAlN and $CrAlSi_{8.6}N$. With an increase in Young's modulus in the coatings, displacement μ_2 did not change. As discussed before, the displacement changed continuously from the coating to the substrate, which could be seen in Fig. 7. There was no change in displacement μ_2 along the thickness of direction in the coating, which meant μ_2 was not caused by the compressive deformation of the coating but by the sinking of the substrate. Because HSS was also a "hard" material with a large Young's modulus, the displacement μ_2 was very small in the current model. There was no displacement on the left side of the coating or substrate in Fig. 7, an indication that there was no residual strain/stress after the indenter slided away. The maximum magnitude of μ_2 in the coatings, $|\mu_2|_{max}$, was 0.1372 for CrAlN, which was slightly larger than 0.1356 for $CrAlSi_{8.6}N$, which have been caused by a larger deformation in CrAlN. Because the spherical indenter was accepted as a rigid body the contact region had the same profile as the spherical surface. Due to the similarity of the displacement μ_2, the contact area was also very similar for CrAlN and CrAlSiN coatings, which could be seen in Fig. 8.

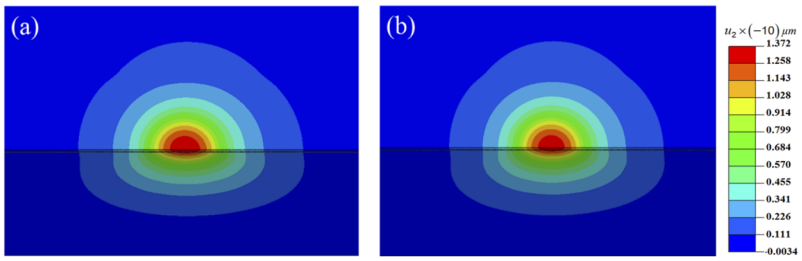

FIG. 7. The distribution of displacement of u_2 on the coating and the substrate for the same region in Fig. 8 for (a) CrAlN and (b) $CrAlSi_{8.6}N$. The maximum magnitude of μ_2, $|\mu_2|_{max}$, was 0.1372 for CrAlN and 0.1356 for $CrAlSi_{8.6}N$ at the contact tip.

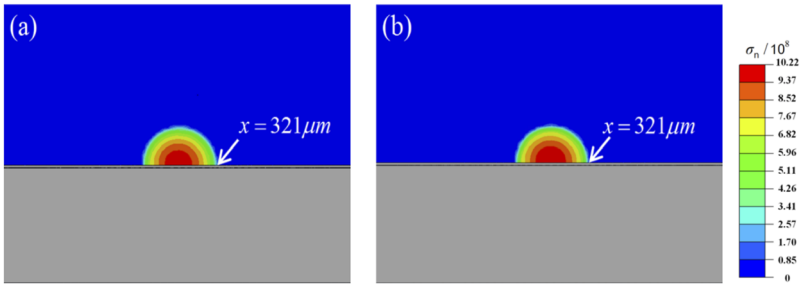

FIG. 8. The distribution of normal contact stress σ_n on the coating for (a) CrAlN and (b) $CrAlSi_{8.6}N$. The maximum of magnitude σ_n was 1.002×10^9 Pa for CrAlN and 1.022×10^9 Pa for $CrAlSi_{8.6}N$.

In Fig. 8, the differences of distributions of normal contact pressure σ_n between CrAlN and CrAlSiN were not obvious and the maximum normal stress σ_n was larger in CrAlSiN because with a smaller Young's modulus, the stress concentration was less severe. The contact radius between the indenter and coating was only around 21 μm but the radius of the indenter was 3170 μm, an indication that the contact surface was almost flat and the contribution of the deformation friction coefficient μ_d was negligible and the scratch friction coefficient μ_s was equal to the Coulomb friction coefficient μ. In the current model, the order of magnitude of the deformation friction coefficient μ_d was 10^{-4}.

While the 3D model was constructed to consider the tribological behavior, there were some challenges which could not be overcomed in the current model or in previous models to simulate the real contact environment. As in Ref. 21, 22, the indenter was assumed to be a rigid body. When the elastic-plasticity material was utilized for the indenter ZrO_2, Figs. 6–8 indicated that the deformation of a sphere would also be elastic and small, because ZrO_2 like HSS was a very hard material. In this case, the small deformation of the indenter would increase the contact area between the indenter and coating, which led to a smaller stress concentration, and further to a smaller effective stress, elastic deformations, and displacements in the coating. However, the use of the elastic-plasticity constitutive for the indenter would draw the same conclusion that the deformation of the coating was completely elastic and scratch coefficient was only from the Coulomb friction coefficient. Secondly, the wear behaviors of the coatings were not taken into account in the models. Fig. 9 shows an increasing scratch friction with number of revolutions, which is due to atomic changes between contact surfaces. Initially, the contact was between ZrO_2 and the coating CrAlN, then between the mixture of ZrO_2 and CrAlN, and CrAlN atoms, and finally between only CrAlN atoms. The Coulomb friction coefficient increased from ZrO_2-CrAlN contact to CrAlN-CrAlN contact, which led to an increasing scratch friction coefficient in Fig. 9 with an increasing number of circles. When the contact was only between CrAlN atoms, the Coulomb friction coefficient (equal to the scratch friction coefficient) did not change, and the curve in Fig. 8 became flat. Similar to hardness, with the increase of Si content from 0 to 8.6 at. %, and then to 13.1at. %, Yong modulus initially grew and then dropped, which would cause the stress concentration to strengthen at first and then weaken. All of the process was Young modulus controlled and the yield strength did not play a role in the scratching in this paper.

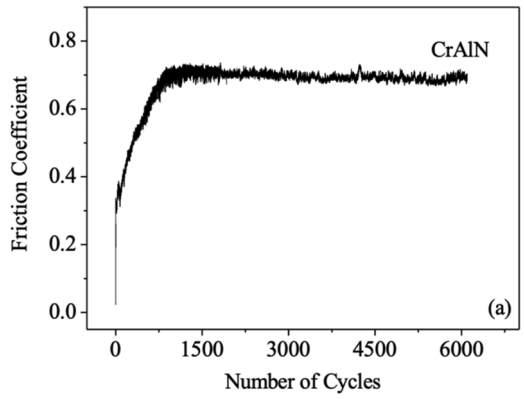

FIG. 9. Friction curves of tested CrAlN film against ZrO_2 ball at room.

V. CONCLUSIONS

The scratch sliding test and FEM modeling were employed to study the tribological behaviors of CrAlSiN coatings at different Si contents. The friction coefficient of CrAlSiN was lower than that of CrAlN coating and the lowest friction coefficient was 0.56 at Si content of 3.7%. The change of friction coefficient could be explained by what were wear scars on the ZrO_2 balls with high Al content having low friction coefficient and tribochemical reaction between Si and ambient humidity. FEM modeling results show that the small elastic deformation took place in the coatings and substrates. The deformation friction coefficient was negligible in comparison with the Coulomb friction coefficient. As increasing Young's modulus, the stress concentration was more obvious in CrAlSiN than in CrAlN.

ACKNOWLEDGMENTS

The authors would like to thank the financial support of the National Nature Science Foundation of China (Grant Nos. 11772302, 10832011 and 11402233) and Public Welfare Technology Application Research Project of Zhejiang Province (2015C31074).

REFERENCES

[1] P. Engel, G. Schwarz, and G. Wolf, Surface and Coatings Technology **112**(1-3), 286–290 (1999).
[2] C. Mello, R. Mansur, N. Santos, W. Viana, and M. Ueda, Surface and Coatings Technology **312**, 123–127 (2017).
[3] R. Wuhrer and W. Yeung, Scripta Materialia **50**(12), 1461–1466 (2004).
[4] B. Tlili, N. Mustapha, C. Nouveau, Y. Benlatreche, G. Guillemot, and M. Lambertin, Vacuum **84**(9), 1067–1074 (2010).
[5] Z. Liu, L. Chen, and Y. Xu, Journal of the American Ceramic Society **101**(2), 845–855 (2018).
[6] C. Zhao, X. Nie, and J. Tjong, ACS Applied Materials & Interfaces **10**(30), 25787–25793 (2018).
[7] Y. X. Xu, C. Hu, L. Chen, F. Pei, and Y. Du, Ceramics International **44**(6), 7013–7019 (2018).
[8] L. He, L. Chen, and Y. Xu, Materials Characterization **125**, 1–6 (2017).
[9] F. Ge, T. Shao, C. Jia, P. Li, and F. Huang, Surface and Coatings Technology **332**, 304–311 (2017).
[10] H. Lee, W. Jung, J. Han, S. Seo, J. Kim, and Y. Bae, Surface and Coatings Technology **200**(1-4), 1026–1030 (2005).
[11] J. Mo and M. Zhu, Tribology International **41**(12), 1161–1168 (2008).
[12] Z. Geng, H. Wang, C. Wang, L. Wang, and G. Zhang, Tribology International **79**, 140–150 (2014).
[13] Y.-Z. Tsai and J.-G. Duh, Thin Solid Films **518**(24), 7523–7526 (2010).
[14] Z. Chen, G. Li, and Y. Xia, Theoretical and Applied Mechanics Letters **2**(2), 7–021007 (2012).
[15] H. Tao, M. Tsai, H.-W. Chen, J. Huang, and J.-G. Duh, Surface and Coatings Technology (2018).
[16] C.-H. Hsu, W.-C. Huang, Y.-P. Lee, and W.-Y. Ho, Surface and Coatings Technology **320**, 230–234 (2017).
[17] Y. Ye, Z. Liu, W. Liu, D. Zhang, Y. Wang, H. Zhao, L. Wang, and X. Li, Tribology International **121**, 410–419 (2018).
[18] R. A. Ibrahim, Applied Mechanics Reviews **47**(7), 209–226 (1994).
[19] J. A. Nairn, S. Bardenhagen, and G. Smith, Computational Particle Mechanics **5**(3), 285–296 (2018).
[20] B. Feng and V. I. Levitas, Journal of Applied Physics **114**(21), 213514 (2013).
[21] B. Feng, V. I. Levitas, and O. M. Zarechnyy, Journal of Applied Physics **114**(4), 043506 (2013).
[22] B. Feng, V. I. Levitas, and Y. Ma, Journal of Applied Physics **115**(16), 163509 (2014).
[23] B. Feng and Z. Chen, AIP Advances **5**(5), 057152 (2015).
[24] J.-L. Bucaille and E. Felder, Philosophical Magazine A **82**(10), 2003–2012 (2002).
[25] K. Holmberg, A. Laukkanen, H. Ronkainen, K. Wallin, and S. Varjus, Wear **254**(3-4), 278–291 (2003).
[26] J. H. Park, W. S. Chung, Y.-R. Cho, and K. H. Kim, Surface and Coatings Technology **188**, 425–430 (2004).
[27] Z. Chen, G. Peng, Y. Xia, and G. Li, presented at the Applied Mechanics and Materials, 2015 (unpublished).
[28] J. Endrino, S. Palacín, M. Aguirre, A. Gutiérrez, and F. Schäfers, Acta Materialia **55**(6), 2129–2135 (2007).
[29] C. Brecher, G. Spachtholz, K. Bobzin, E. Lugscheider, O. Knotek, and M. Maes, Surface and Coatings Technology **200**(5-6), 1738–1744 (2005).
[30] S. Vepřek and S. Reiprich, Thin Solid Films **268**(1-2), 64–71 (1995).
[31] C. Lin and J. Duh, Surface and Coatings Technology **204**(6-7), 784–787 (2009).
[32] A. Lasalmonie and J. Strudel, Journal of Materials Science **21**(6), 1837–1852 (1986).
[33] S. Tao, Z. Yin, X. Zhou, and C. Ding, Tribology International **43**(1-2), 69–75 (2010).
[34] B. Feng and V. I. Levitas, Materials Science and Engineering: A **680**, 130–140 (2017).
[35] B. Feng and V. I. Levitas, International Journal of Plasticity **92**, 79–95 (2017).
[36] S. K. Kim, V. Van Le, P. Van Vinh, and J. W. Lee, Surface and Coatings Technology **202**(22-23), 5400–5404 (2008).
[37] I.-W. Park, D. S. Kang, J. J. Moore, S. C. Kwon, J. J. Rha, and K. H. Kim, Surface and Coatings Technology **201**(9-11), 5223–5227 (2007).
[38] H. Jiang, G. Lim, J. Reddy, J. Whitcomb, and H. J. Sue, Journal of Polymer Science Part B: Polymer Physics **45**(12), 1435–1447 (2007).
[39] K. Holmberg, H. Ronkainen, A. Laukkanen, K. Wallin, S. Hogmark, S. Jacobson, U. Wiklund, R. M. Souza, and P. Ståhle, Wear **267**(12), 2142–2156 (2009).
[40] S. Chen, B. Feng, Y. Wei, and T. Wang, International Journal of Solids and Structures **48**(21), 3099–3111 (2011).
[41] S. V. Hainsworth and W. Soh, Surface and Coatings Technology **163**, 515–520 (2003).